energies

Article

Impact Tests and Computed Tomography Scans of Prismatic Battery Cells

Simon Schwolow [1,2,*], Muhammad Ammad Raza Siddiqui [1,2], Philipp Bauer [3] and Thomas Vietor [2]

[1] Research and Development, Volkswagen AG, VW-Straße 103, 38440 Wolfsburg, Germany
[2] Institute for Engineering Design, Technische Universität Braunschweig, Hermann-Blenk-Straße 42, 38108 Braunschweig, Germany
[3] TUEV SUED Battery Testing GmbH, Daimlerstraße 15, 85748 München, Germany
* Correspondence: simon.schwolow@volkswagen.de; Tel.: +49-5361-986-751

Abstract: Recently, the use of prismatic cells in electric vehicles has increased significantly. Unlike the cylindrical or pouch format, the prismatic cell format has not been sufficiently investigated. In this study, quasi-static mechanical tests are performed on prismatic cells. The tests include a cylindrical and a hemispherical impactor that mechanically load the cells in all three spatial directions. In both in-plane directions, a cell stack consisting of three cells is tested to capture the influence and loading of the outer cells of a cell stack. It is found out that, in the in-plane tests, short-circuiting occurs first in the outer cells and subsequently in the middle cell, which is targeted by the impactor. This result can also be supported by computed tomography scans. The results illustrate that, when evaluating the crash safety of battery cells, several cells should always be tested in order to capture the different loading of the cells.

Keywords: prismatic cell; crush test; cell stack; cylindrical impactor; hemispherical impactor; computed tomography

check for updates

Citation: Schwolow, S.; Siddiqui, M.A.R.; Bauer, P.; Vietor, T. Impact Tests and Computed Tomography Scans of Prismatic Battery Cells. *Energies* **2022**, *15*, 8330. https://doi.org/10.3390/en15228330

Academic Editor: Fangming Jiang

Received: 10 October 2022
Accepted: 3 November 2022
Published: 8 November 2022

1. Introduction

In recent years, the number of electric vehicles on the road has continued to increase. The battery of an electric vehicle can pose a fire risk in the event of a vehicle crash. To reduce this risk, the mechanical properties of the battery must be known so that the car body can be matched to the battery to be protected. With a matched body, the battery can be protected in a vehicle crash so that the fire risk remains low. In the past, there has been some research on the mechanical properties of a lithium-ion battery. Since many electric vehicles are equipped with cylindrical or pouch cells, these cell formats have been studied extensively. For example, a directional dependence of the mechanical properties due to the layered structure within a battery cell could be found [1–4]. When a cell is loaded in the out-of-plane direction, the load is primarily absorbed by the active materials, which can be compressed like a foam [5–9]. However, when a cell is loaded in the in-plane direction, the current collector foils come into play and the individual layers bulge and buckle [10–12]. It was also found that the mechanical failure of a battery cell coincides in time with the occurrence of a short circuit [13–15]. After a short circuit, a thermal runaway can be triggered especially at a high state-of-charge (SOC) of a battery cell [16,17]. Both the electrolyte and the gases generated inside the cell can be flammable [18,19].

Meanwhile, prismatic cells are increasingly being installed in electric vehicles, which is why this cell format is also being investigated. Prismatic cells with a capacity of 63 Ah were loaded both statically and dynamically in [20]. The loading direction was limited to the out-of-plane direction. In the study by Zheng [21], only the out-of-plane direction was considered as well, and the cells had a capacity of 5 Ah. In the study of Zhu et al. [22], all directions were tested, both quasi-statically and dynamically. Prismatic cells with a capacity of 234 Ah were used in the experiments. Both out-of-plane and in-plane, only one cell was tested in each piece of experiment. Prismatic cells were quasi-statically and dynamically tested in two of the three spatial directions in [1]. In the study of Xiao et al. [23], the lateral in-plane direction was analyzed. Prismatic cells with a capacity of 50 Ah were quasi-statically and dynamically loaded both with and without a lateral support. The investigations described always used one cell per test. It is assumed that, especially in the in-plane direction with larger impactors, it is important to also examine the neighboring cells, since each cell is loaded differently. In the study of Deng et al. [24], this is realized as a prismatic module consisting of five cells with 63 Ah capacity each being tested. All tests were carried out dynamically.

This leaves open how several cells behave under in-plane loading without additional components of a module such as the side- or endplates. Another aspect to be investigated with this work is the influence of the impactor on the intrusion tolerance. Various studies can be found in the literature, which also test different impactors. For example, in [14], the intrusion tolerance was compared between a spherical and a wedge impactor. In contrast, in [25], the influence of different diameters of a spherical impactor was evaluated. However, there is no comparison between spherical and cylindrical impactors with the same diameter for experiments in all spatial directions. The addressed gaps shall be filled with this research. In this study, prismatic cells are loaded with different impactors in the in-plane and out-of-plane directions. In the in-plane direction, three cells are tested at a time to investigate the consequences for all loaded cells.

2. Materials and Methods

Prismatic cells with a capacity of more than 100 Ah are investigated. An overview of the tested configurations can be seen in Table 1. All spatial directions are tested with different impactors. The configurations are intended to simulate possible loads of a real car crash accident. In the study of Kalnaus et al. [26], a battery module consisting of several pouch cells was loaded in an out-of-plane direction. The test results and computed tomography scan (CT scan) have shown that all jellyrolls within the module exhibit similar deformation patterns and that a short circuit occurs first in the cell near the impactor. Therefore, only one cell is tested at a time in the u-direction (out-of-plane) in this work. In the v- and w-direction (in-plane), three cells are always tested in order to also investigate the effects on the neighboring cells. The cells in v- and w-direction are supported laterally. This support is intended to be rigid. Both the hemispherical and cylindrical impactors have a diameter of 100 mm. The cells at test have a state-of-charge (SOC) of 100%. All tests are performed quasi-statically at a velocity of 1 mm/s. Real crash accidents are dynamic and can cause much higher velocities. For dynamic tests, especially drop tower tests, it is difficult to precisely define the intrusion of the impactor. In order to examine the tested cells after the test with computed tomography, it had to be ensured in this work that a certain intrusion is not exceeded. Hence, a velocity of 1 mm/s is chosen for the impactor.

A change of the impactor always requires a lot of time. Therefore, all tests are first performed with the hemispherical impactor and then all tests with the cylindrical impactor. Finally, the bending test is performed in the u-direction. Table 1 also shows the short names of all the tests. The configuration with hemispherical impactor in v-direction was tested four times because QT03 and QT04 were unusable for data acquisition.

Table 1. Test configuration in u-, v-, and w-directions.

Impactor	U-Direction		V-Direction		W-Direction			
Hemispherical (Ø100 mm)	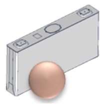	QT01, QT02	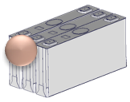	QT03, QT04, QT05, QT06	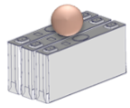	QT07, QT08	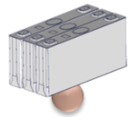	QT09
Cylindrical (Ø100 mm)	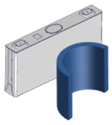	QT10, QT11, QT12	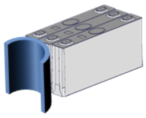	QT13, QT14		QT15, QT16		
Cylindrical (Ø100 mm) Three-point Bending	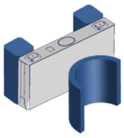	QT18			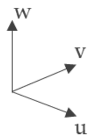			

All tests were carried out at TUEV SUED Battery Testing GmbH. The test setup is described in Figure 1. This figure shows test QT01, in which a cell is loaded in u-direction with the hemispherical impactor. The hemispherical impactor is forced into the cell by means of a compression test rig. The impactor itself is wrapped with Kapton and insulating tape to prevent the impactor from short-circuiting the cell. The displacement of the impactor is measured by a linear potentiometer. Three load cells attached to the back panel of the impactor measure the force during the experiment. Three video cameras record the experiment from different perspectives. Photo cameras record all the important details both before and after the experiment. These images are important later for comparison with a simulation model. For each cell, the temperature and voltage are measured at three points. The temperature is measured at the positive terminal, at the negative terminal and at the vent. The voltage is measured first between the positive and negative terminals of the cell. In addition, the voltage is measured between the positive terminal of the cell and the impactor and between the negative terminal of the cell and the impactor. This is to check whether the insulation of the impactor remains intact during the test.

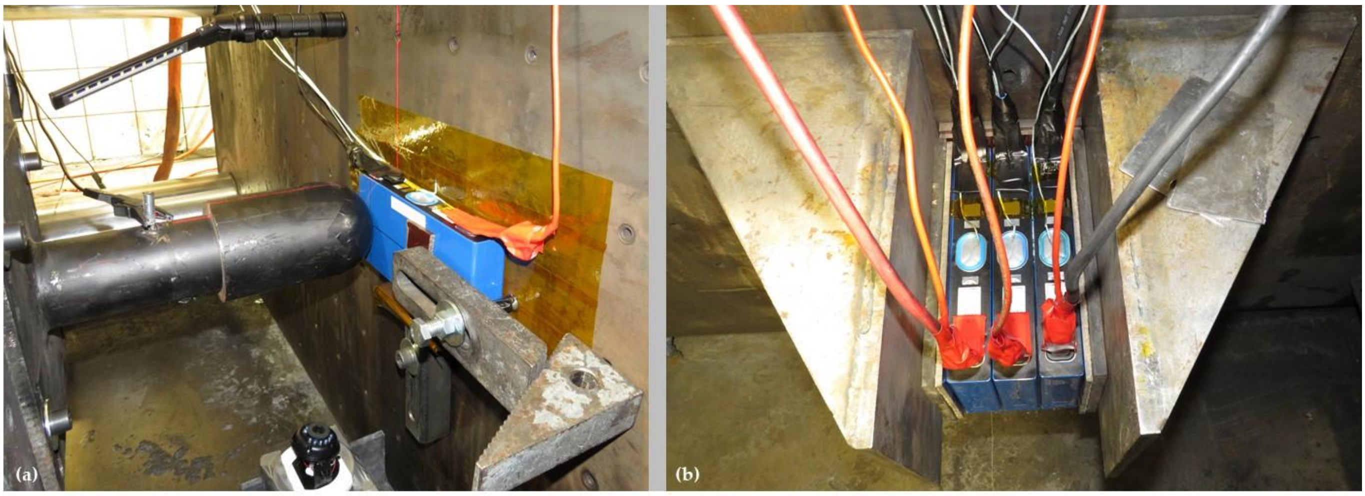

Figure 1. Test setting for static crush test (**a**) u-direction with one cell; (**b**) v-direction with three cells.

The tests were performed as follows: for each configuration, the first test is executed until the event. In this study, event always means a venting of the cell, which also resulted in a fire in all tests. The last test of each configuration is then no longer executed until the event but stopped beforehand. After a 30-min observation period, the deformed cell is then discharged and short-circuited so that it can be examined with a computed tomography scan.

3. Results

The evaluation of the voltage measurement between the impactor and the cells shows that the impactor did not trigger a short circuit in any test. In some tests, contact of the impactor to one of the terminals was detected, but never to both terminals. In the following, the directions are evaluated individually. Force, displacement, cell voltage, and temperature curves are evaluated, with special mention of new findings.

3.1. u-Direction (Out-of-Plane)

In Figure 2, the results for the u-direction are plotted. Due to confidentiality of prototype test data, axes are shown without numerical values. Exact numerical values are not necessary for this investigation, since the comparison between the impactors, the description of the curves, and the evaluation of the scatter between the experiments can be conducted without exact numerical values. The cylindrical impactor causes a significantly higher force than the hemispherical impactor. This was already expected due to the larger contact area of the cylinder. All curves are initially bent and then become linear. Finally, it is particularly noticeable in the three tests with cylinder impactors that the tests scatter only a very little amount. On the one hand, this is due to the measurement technique, but, on the other hand, it is also due to the fact that the tested cells all correspond to an advanced prototype status. This means that the difference between the individual cells is negligible due to high production standards. In Figure 2, a red triangle indicates when an event occurred during a test. The marker is set after the cell voltage drop in all representations. For the u-direction, cell voltage drop and force drop coincide closely.

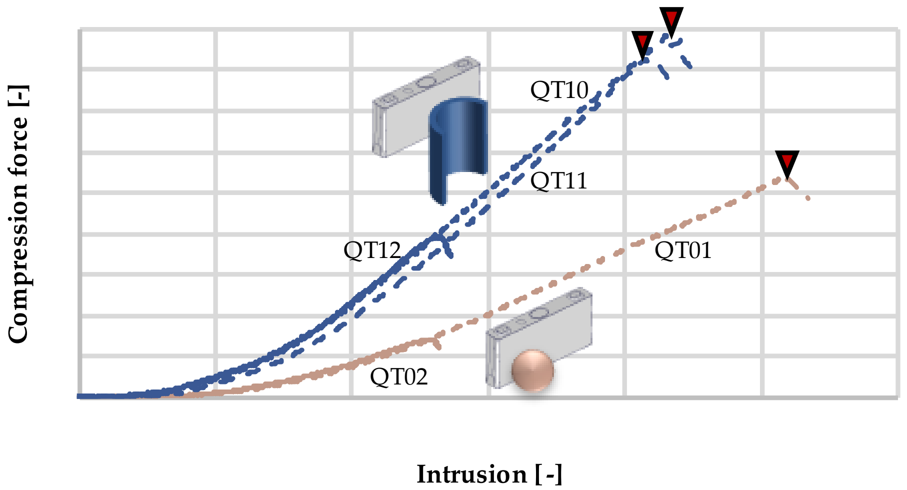

Figure 2. Compression force over intrusion in u-direction.

Figure 3 shows the test data for the first test QT01. The upper part shows the force and cell voltage over time. Due to confidentiality of prototype test data, the time is only shown as a time period without any unit. The drop in force and the drop in cell voltage coincide closely. However, it is noticeable that the cell voltage does not drop completely but rises again slightly in the meantime and it takes a total of approx. 1 time period for the cell voltage to drop entirely. It is assumed that, due to the size of the cell, only a part of the layers was deformed and a large part remained intact until the fire affected the entire cell.

In the lower part of Figure 3, the temperature measured at the positive and negative terminals and at the vent is shown along with the force. Shortly after the drop in force, the temperature at the negative terminal and at the vent rises very sharply. The temperature at the positive terminal, on the other hand, rises much more slowly. This is attributed to the fact that the impactor has been pushed into the cell below the negative terminal and has probably also triggered a short circuit in that region.

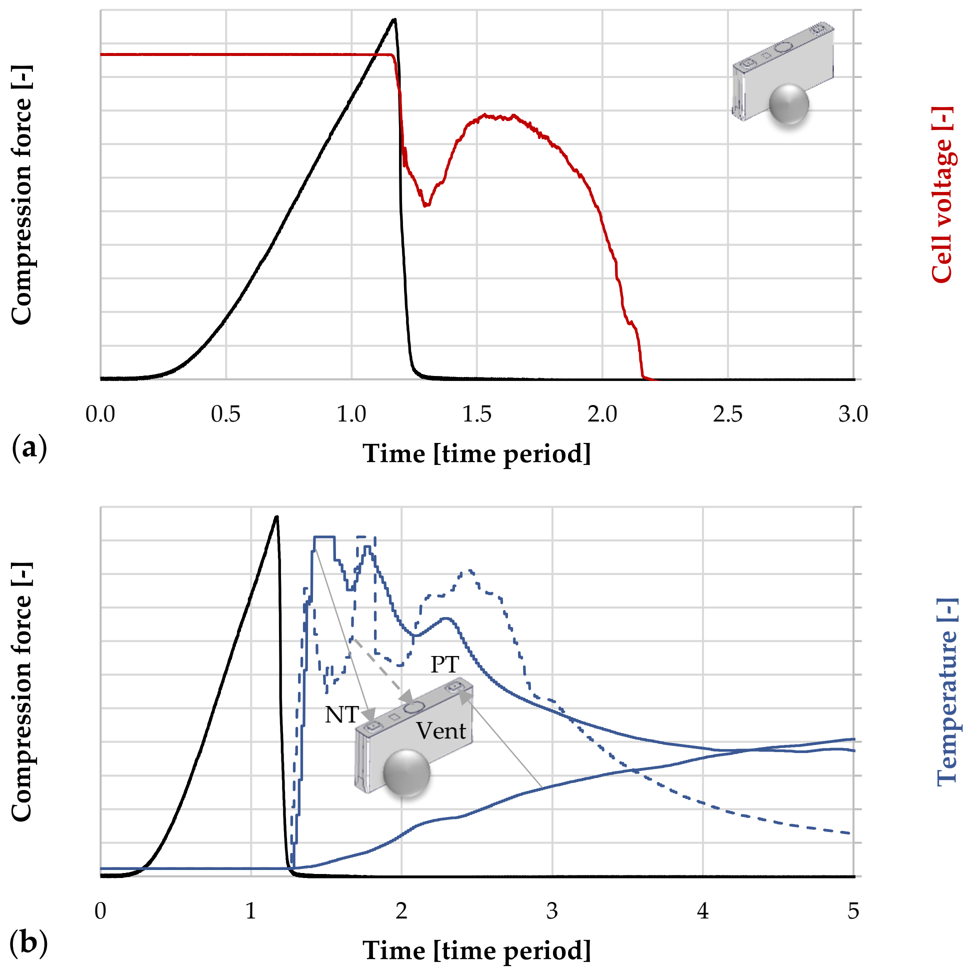

Figure 3. Test data of test QT01: (**a**) compression force and cell voltage over time; (**b**) compression force and temperature over time (NT: negative terminal, PT: positive terminal).

In addition, in u-direction, the difference in the tests with cylindrical impactor and different support is interesting. Tests QT10, QT11, and QT12 were performed with a rigid barrier behind the cell. In test QT18, the cell is loaded by a three-point bending: the cylinder also enters the cell in the middle, but the cell is only supported by two square beams (50 mm $\times$ 50 mm), which have a corner radius of 7 mm. To illustrate the difference between these two load cases, the intrusion and the cell voltage versus time period are plotted in Figure 4. In test QT10, the cell voltage already drops at a low intrusion. In this load case, the layers are compressed by the cylindrical impactor until a short circuit occurs. In test QT18, the cell can tolerate around eight times more intrusion. The cell voltage drops here at a high intrusion. The videos of the experiment show that the cell makes contact with the rigid support during bending. The contact point is marked on the curve in Figure 4. From this point on, the individual layers are also compressed in this load case and, after a small additional intrusion, the cell voltage drops. Another difference between the two load cases is the drop of the cell voltage. In test QT10, the cell voltage drops rapidly, while, in test QT18, it takes more than one time period for the cell voltage to drop completely.

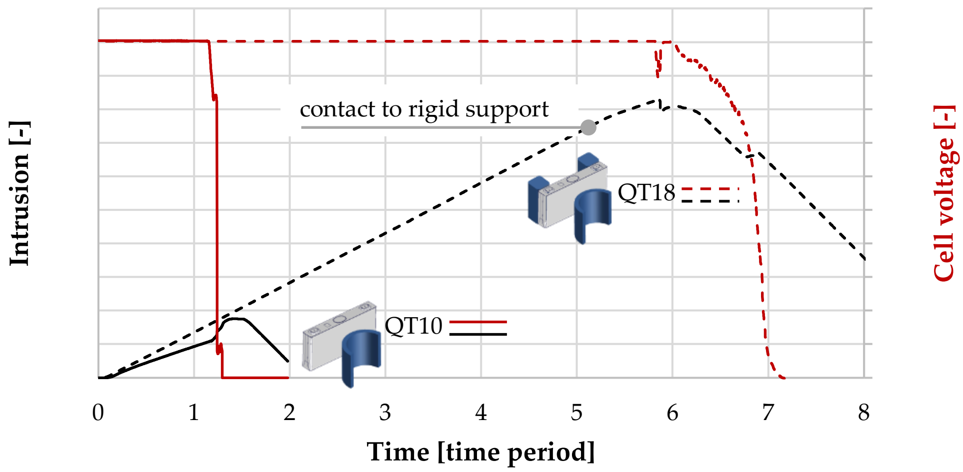

Figure 4. Intrusion and cell voltage over time for two test configurations: QT10—cylindrical impactor with rigid support and QT18—cylindrical impactor with three-point bending.

3.2. *v-Direction (In-Plane)*

Figure 5 shows the evaluation of force versus intrusion for the v-direction. In this direction, too, both tests with cylindrical impactor are above the curves with hemispherical impactors. The two curves with cylinders show clear differences. The first test with cylinder was executed until the impactor almost touched the lateral support. However, there was no event in this test. Therefore, the support had to be slightly shortened to allow the impactor to move further into the cell stack on the second trial to determine the event limit. The support was lessened in the region of the impactor hit, giving the cells more room to expand in the direction of the stack. This results in a decrease of stiffness at QT14. It is also noticeable that the event occurs significantly earlier with the hemispherical impactor than with the cylindrical impactor.

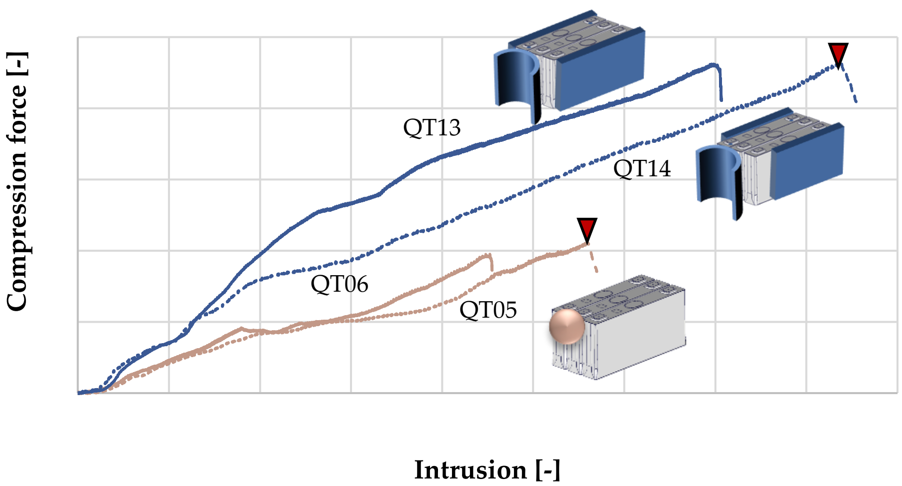

Figure 5. Compression force over intrusion in v-direction (red triangle mark event. No triangle, no event).

In the v-direction, it is also interesting to see at which cell an event occurs first. Figure 6 shows both the force and the cell voltage over time. The cell voltage of the middle and the right cell is shown. The cell voltage of the left cell remains constant in the depicted time range; this is why the curve is not shown. The force increases from the beginning up to approx. the 2.6 time period, after which the force drops abruptly. The drop in force is accompanied by a drop in cell voltage at the right cell. However, the drop in cell voltage is not as strong as the drop in force; it takes about 1 time period for the cell voltage of the right cell to drop completely. At first sight, this is surprising, since the event already takes place at the first dip at approx. a 2.6 time period in the video, and a fire can be clearly seen. The fact that it still takes around 1 time period for the cell voltage to drop completely could be related to the size of the cell. At this point, it is assumed that many layers are still intact at the start of the event that a voltage is still present between the positive and negative terminal.

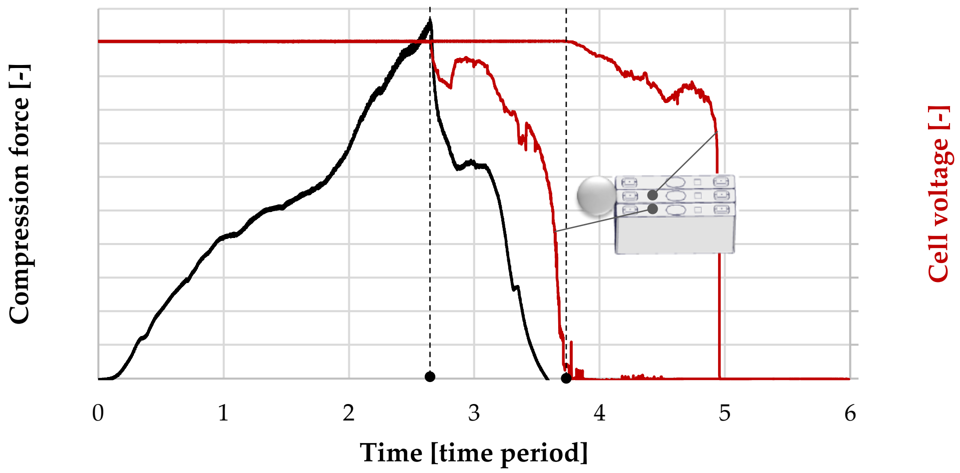

Figure 6. Compression force and state of charge over time for middle and right cell at test in v-direction with hemispherical impactor.

All data of the experiments in v-direction show that the first event occurs—in each experiment with event—in one of the outer cells. What differs between the tests is the time between the first event in one of the outer cells and the next event. The shortest interval is about 0.5 time period, and the largest interval is about 1 time period.

In order to find the reason why an event occurs first in the right cell, Figure 7 is considered. The deformed cells after experiment QT06 show that the middle cell expands to both sides. It is assumed that this lateral expansion puts additional stress on the neighboring cells. A further analysis is made with the CT scans.

Figure 6 also shows how long it takes for the cell voltage to drop at the middle cell. The interval between the drop in the cell voltage of the middle and right-hand cells is approx. 1 time period. It is important to note that the impactor continues to intrude for a short time after the drop in force, but only up to 3.2 time period. After that, the impactor retracted, which is why it is assumed that the middle cell reached the thermal runaway due to the heat of the right cell and not due to mechanical deformation. To verify this, the temperature sensors of the middle and right cell on the vent are evaluated. In addition, an image at 2.7 time period has been taken from one of the video recordings. Both can be seen in Figure 8. In the upper left corner of the image, the beginning of the event with fire can be seen. In addition, the temperature sensor on the vent of the right cell can be recognized at the bottom of the image. The temperature sensor on the vent of the middle cell is hidden in this picture. The short-circuit in the right cell causes both temperature measurements to increase from 2.7 time period onwards. The temperature of the right cell at the vent even rises somewhat faster, which was also expected due to the short circuit.

Figure 7. Deformation of cells after test QT06 (v-direction hemispherical impactor), (**a**) at test rig, (**b**) middle cell after test and (**c**) right cell after test.

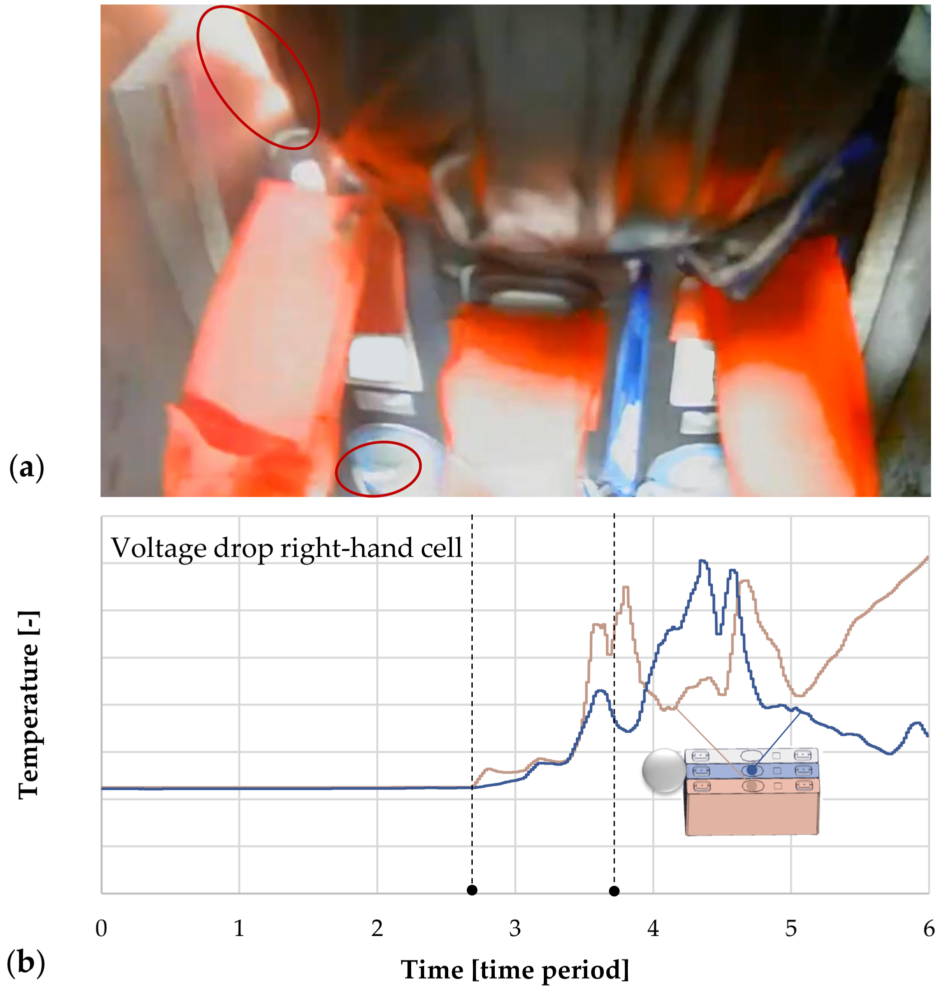

Figure 8. (**a**) V-direction with hemispherical impactor at event; (**b**) temperature over time for sensor at vent.

3.3. w-Direction (In-Plane)

Finally, the curves of the tests in the w-direction are evaluated. Force versus intrusion is shown in Figure 9. The curves of the tests pushed from above both show a curved course. With the cylindrical impactor, a clear increase can be seen at the beginning, but afterwards the curves level out somewhat. This can be attributed to the support in the two configurations. Although the cylindrical impactor has a larger contact area and therefore a greater increase in force at first, the support for the cells is open in the middle so that the cylinder can move into the cells. This makes it possible for the cells to move out of the way. On the other hand, in the test setup for the hemispherical impactor, the cells are fully supported at the sides, which means that the force increases only slightly at first, but then steadily. If one compares only the tests from above, then here too, like the v-direction, the event clearly takes place earlier with the hemispherical impactor. Only when the hemispherical impactor pushes from below does the event occur later.

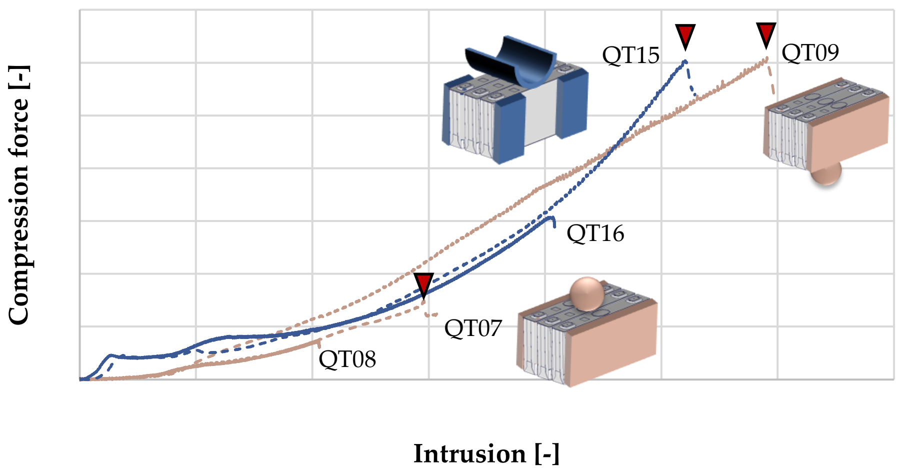

Figure 9. Compression force over intrusion for tests in w-direction.

In w-direction, it is also investigated at which cell an event occurs first. For this purpose, test QT07 is analyzed in more detail, in which the hemispherical impactor pushes into the cells from above. Figure 10 shows force and cell voltage versus time. The cell voltage is only shown from the middle and right cell, since the cell voltage of the left cell does not change in the time range shown. Between the start and 1.6 time period, the force increases steadily. From 1.6 time period, the force drops sharply and the cell voltage of the right cell also initially shows a smaller drop. From 2.3 time period, the cell voltage then drops completely. From the first drop in cell voltage of the right cell to the first drop in cell voltage of the middle cell, the 3.8 time period elapses. Only at approximately the 5.4 time period does the cell voltage of the middle cell begin to drop slowly, and, from approx. the 6.5 time period, it then drops completely. A similar pattern is also discovered in the other experiments in the w-direction where an event has occurred. In one of the outer cells, an event occurs first and then it takes some time for the middle cell to reach thermal runaway. For the load case with the hemispherical impactor from below, the interval is 2 time period, for the load case with the hemispherical impactor from above, it is a 3.8 time period, and, for the load case with the cylindrical impactor, it is a 37 time period. The fact that the time for the load case with cylindrical impactor is significantly greater than for the other two load cases is attributed to the support, which was not continuous in this load case to allow the cylinder to move into the cell stack. As a result, the cells diverge strongly due to the deformation and the heat can be released to the environment more easily.

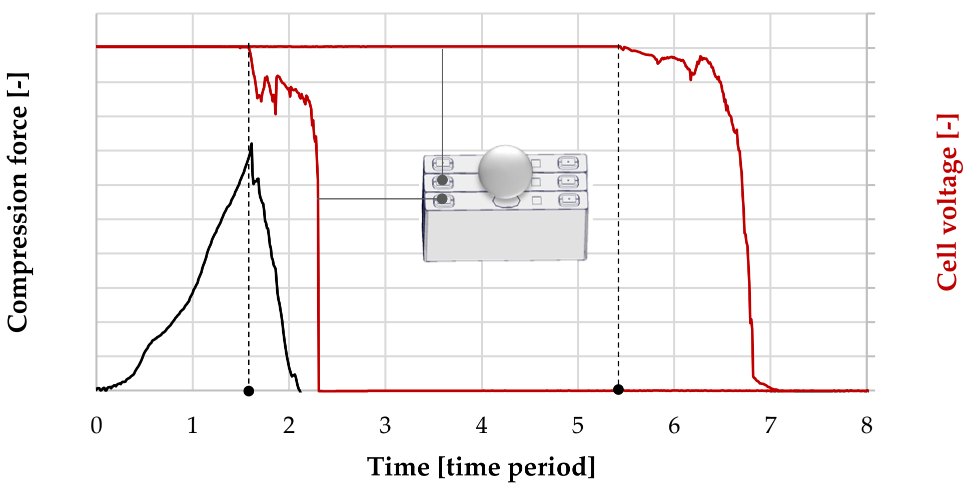

Figure 10. Compression force and state of charge over time for middle and right cells at test in w-direction with hemispherical impactor.

3.4. Evaluation of CT-Scans

To understand the failure mechanisms of the battery cells during the different abuse scenarios, it is very essential to investigate the mechanical behavior of the battery cells. Therefore, the CT-Scans of the battery cells involved in the abuse tests have been carried out and the interesting and relevant findings of the CT-Scans follow. All CT-Scans were performed with a resolution of 70 µm. With this resolution, a section of approximately 60 mm of the battery cell could be analyzed.

Figure 11a shows the deformed cell in u-direction, which was loaded with a hemispherical impactor. A pictogram of the load case can be seen in the lower right corner. Figure 11b shows a uv-plane scan of the deformed cell. In the lower right corner, the pictogram shows the scanned section in red. The representation with the pictograms for the load case and the scanned section is adopted for the following figures. In Figure 11a, the deformed cell and the imprint of the impactor can be seen. In Figure 11b, it is obvious that the active materials of the jellyroll have been compressed. The thickness of the individual jellyroll segments is compared to the undeformed thickness. The difference is between 5% and 9% of the original thickness. Due to the static load case, an even distribution is expected. However, the deviations can be explained by the limitation of CT-scans resolution (70 µm). An exact selection of the jellyroll segments is not always possible, and the measured values differ.

The compression of active materials also elaborates the decrease in porosities of active materials, which resulted in squeezing out the electrolyte from the active materials, hence endorsing the nonlinear behavior of the jellyroll under compression as reported in Figure 2.

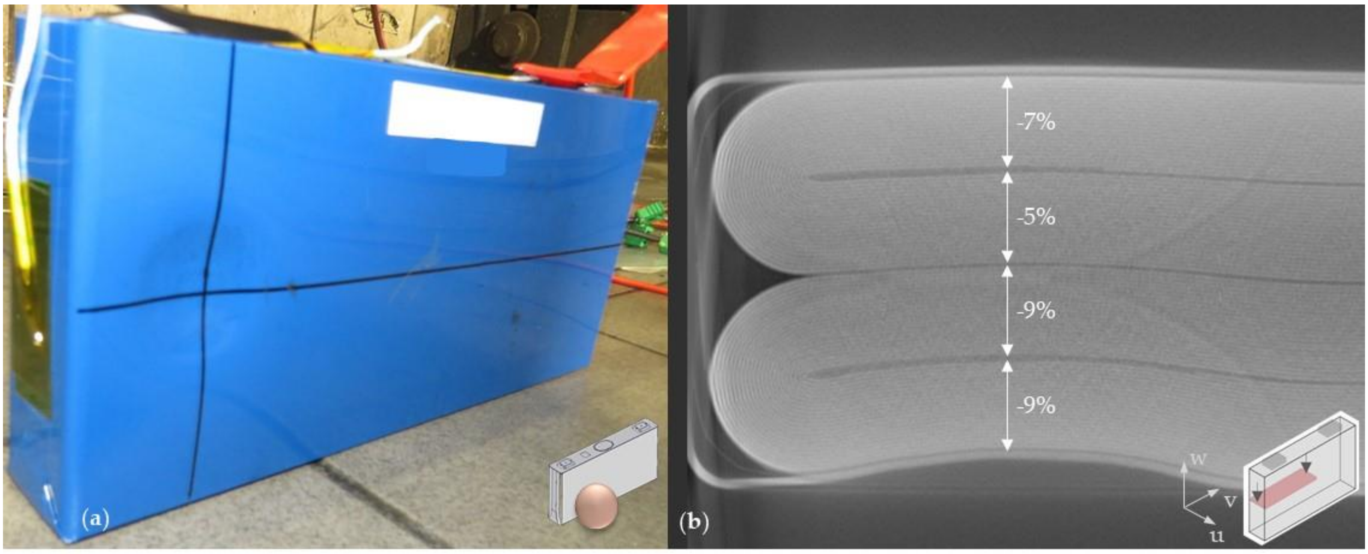

Figure 11. U-direction with hemispherical impactor: (**a**) deformed cell; (**b**) CT-Scan at uv-plane.

In addition, Figure 12 shows (a) the deformed cell and (b) the CT-Scans at uw-plane of compression test with a cylindrical impactor. The cross-section of CT-Scans in Figure 12b illustrates that the cell casing is plastically deformed at the top and the bottom. However, due to the impactor height, plastic deformation over the whole casing height was expected. The difference can be explained by the behavior of the electrodes, which seems to be only elastically compressed. Therefore, the deformation in the middle of the cell casing regresses. In contrast, at the top and bottom, the casing was plastically deformed, and this deformation is still visible.

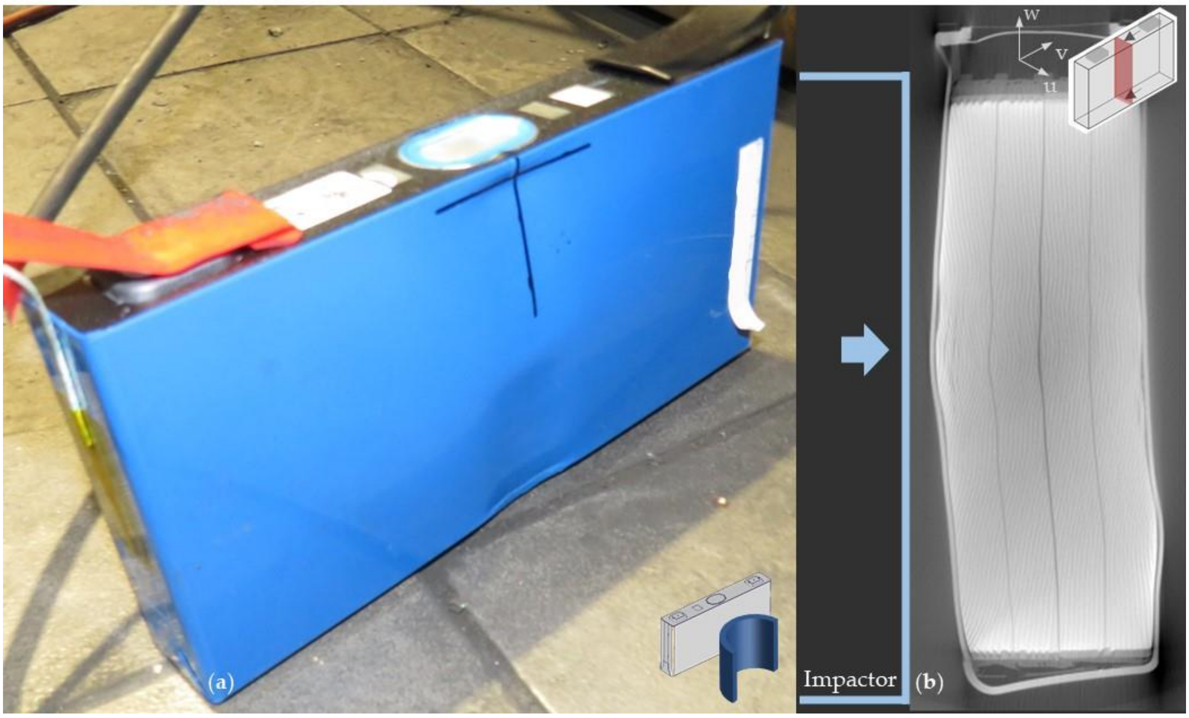

Figure 12. U-direction with cylindrical impactor: (**a**) deformed cell; (**b**) CT-Scan at uw-plane.

Similarly, the CT-Scans of v-directional abuse tests are of special interest to reveal the initiation of short circuit, mechanical integrity of the cell casing as well as jellyroll, failure of separator and condition of welding joints at the current collector tabs.

First, the CT-Scans of the middle cell involved in the v-directional hemispherical indentation test were captured as shown in Figure 13. Figure 13a illustrates the deformed condition of the battery cell where an opening of the casing can be seen, which resulted in leakage of electrolytes during the abuse experiment. Furthermore, a sharp bend can be observed at the center of the battery cell casing; therefore, it is quite important to investigate the jellyroll in that region. Figure 13b reveals that the layers of the jellyroll seriously bulge at the middle of the cell but are different from the casing deformation.

Likewise, the horizontal cross-section near the loading position in Figure 13c possesses a similar trend, where it can be seen that the layers of electrodes are extremely bulged, but there is no sign of the development of cracks within the layers. In addition, there is no drop of cell voltage in the test data, which confirms that there is no failure of layers of jellyroll. Nonetheless, sharp kinks can be seen as well as delamination of layers. Furthermore, the current collector tabs are also examined through the CT-Scan process to detect the condition of electrical weld joints as shown in Figure 13d. It is found out that the joints were in contact with the tab, and the test data of cell voltage also validates this finding.

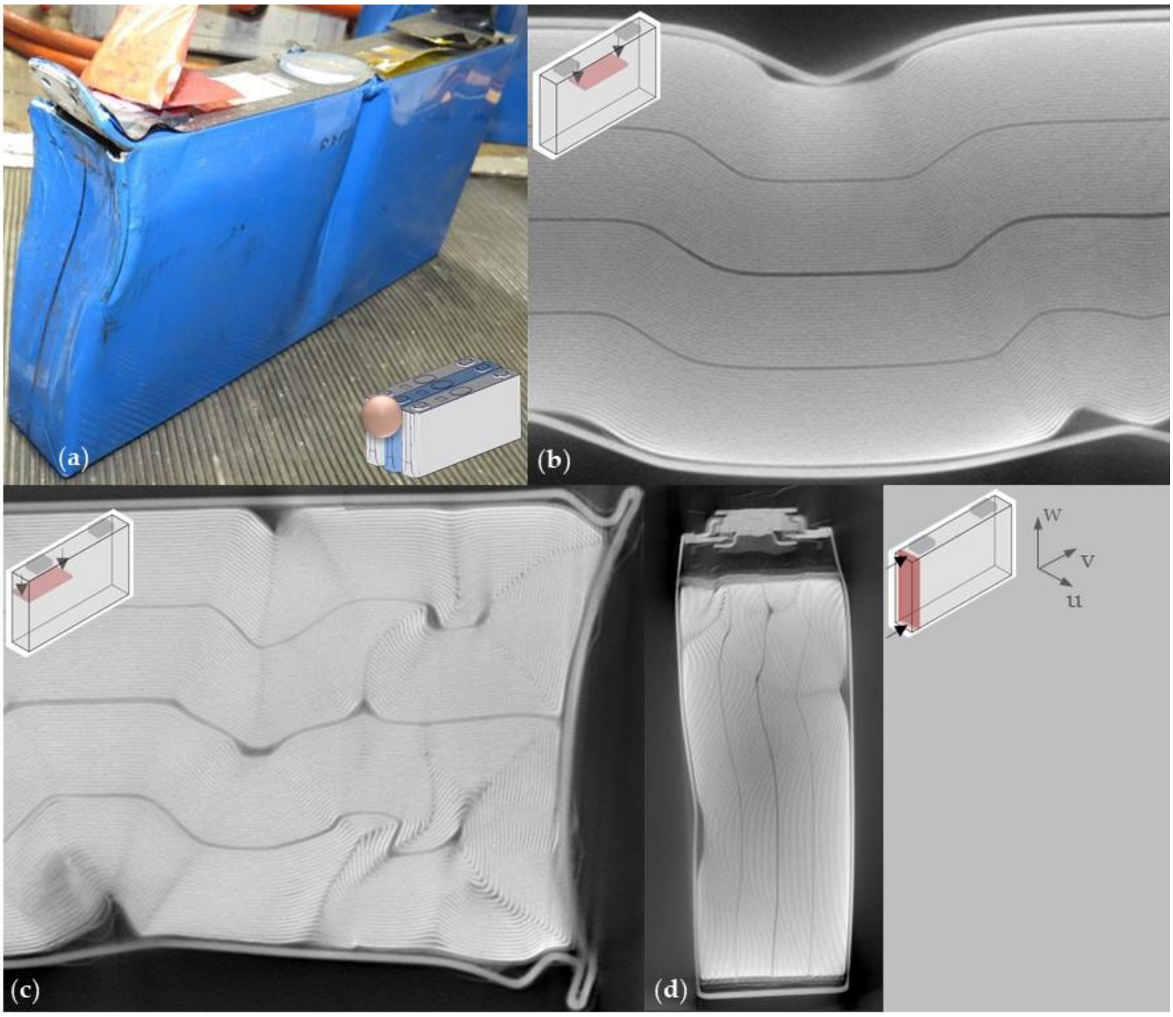

Figure 13. V-direction with hemispherical impactor: (**a**) deformed middle cell; (**b**–**d**) CT-Scans.

In addition, the left cell of v-directional hemispherical indentation test is depicted in Figure 14. Figure 14a shows the deformed cell with the opened casing at the loading position. In all CT scans in Figure 14b–d, a clear crack in the jellyroll is visible. With Figure 14d, the difference in loading between the two jellyrolls of the cell is apparent. The inner one near the impactor shows deformation and bulge, while the outer one seems to be almost unloaded. In Figure 14c, a scan in vw-plane is depicted. In the upper part of the jellyroll where the cell is loaded by the impactor, the jellyroll is deformed and pushed inside the cell. In contrast, the lower part of the jellyroll seems to have the origin position as before the test. In the transition region, the crack is apparent, which leads to the assumption that this crack is caused by tension loading of the layers through the different load force at the upper and lower part of the jellyroll. Although the crack is clearly visible, no cell voltage drop was measured during the test. Therefore, it is assumed that the separator layers in the jellyroll remain intact, hence only the physical contact of electrodes leads to short circuit. Again, the tabs of the cell were examined to inspect the electrical contacts, and Figure 14c provides the evident demonstration of the integrity of the electrical connections, as neither the current collector tears off nor the welded connection torn from the current collector.

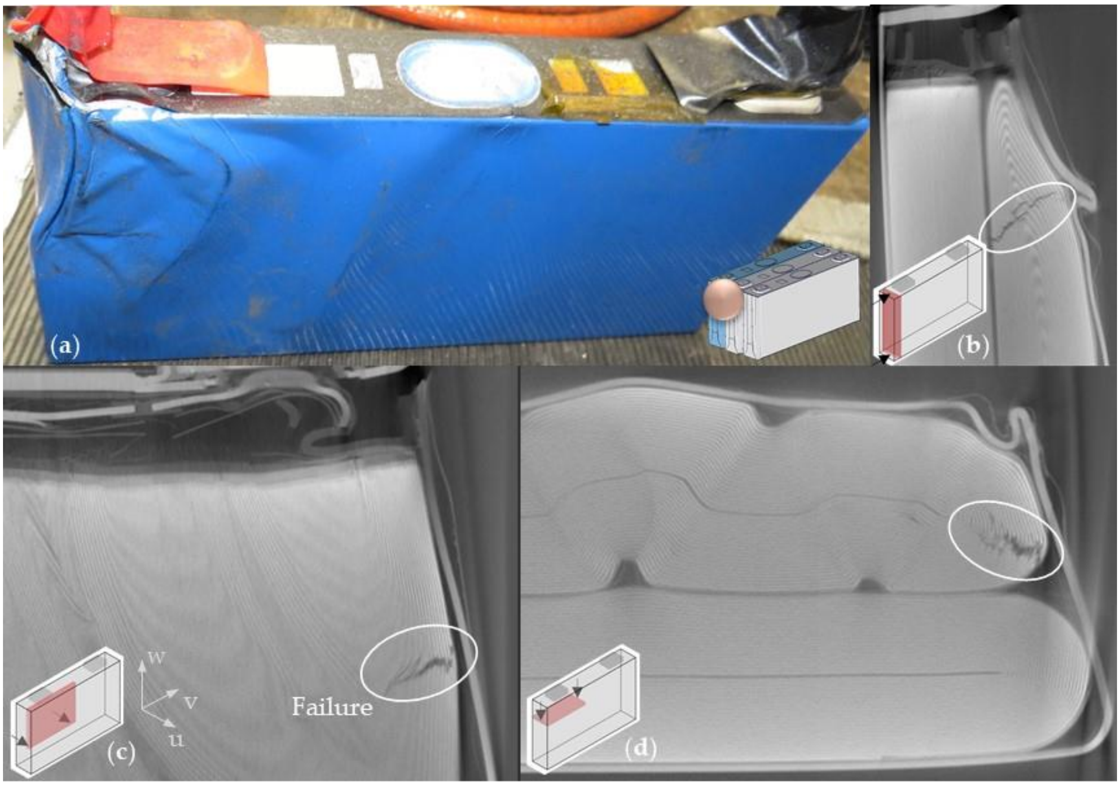

Figure 14. V-direction with hemispherical impactor: (**a**) deformed left cell; (**b**–**d**) CT-Scans.

Furthermore, CT-Scans of battery cells incorporated in a v-directional cylindrical compression test were carried out. Figure 15 depicts the different cross-sections of the middle cell at certain locations. At first, the CT-Scans in uw-plane in Figure 15b,c near the current collector tab highlights the significant rapture of several layers of electrodes at the bottom. From Figure 15a, one can also notice that the battery cell casing is severely damaged in the region close to the safety vent, as the buckling of the casing took place. Therefore, it is necessary to investigate the CT-Scans of jellyroll in the region of the safety vent and yet again the serious failure of electrode layers can be seen in Figure 15d. Figure 15e also contains the CT-Scans of the battery cell near the impacted region, which unveils the buckling and delamination of the electrode layers.

The right cell involved in the cylindrical compression test in v-direction was also examined through CT-Scans. Figure 16a shows the deformed cell with the opened casing near the impactor and the buckled casing caused by the deformation. Figure 16b shows the section view in uv-plane close to the impacted region, where the failure of electrodes layers is quite evident. Similarly, another section view in the same region illustrates in Figure 16e the phenomenon of delamination of electrode layers. However, the experimental data of cell voltage shows no drop, even though the failure of electrodes was quite predominant. In addition, with Figure 16b,e, the different loading of the two jellyrolls is apparent. While the jellyroll near the impactor shows buckling and delamination, the outer one shows nearly no deformation except for the failure near the cell casing.

On the other hand, the CT-Scans of the current collector tabs indicate in Figure 16 c,d that the electrical connections were almost intact; this could be the obvious reason for no drop in cell voltage. However, a small part of the yellow marked current collector shows failure. In Figure 5, it was quite interesting to observe that the battery cells involved in hemispherical indentation tests failed earlier by withstanding less resistance against the impact compared to the cylindrical compression test. The reason for this could be that the jellyroll during a hemispherical indentation test experienced tension as the hemispherical impactor was only indenting the topmost area of the cell, and the rest of the jellyroll was not affected by the impacted load. On the other hand, in the cylindrical compression test, the complete jellyroll is under compression, and there would be no tension force within the layers.

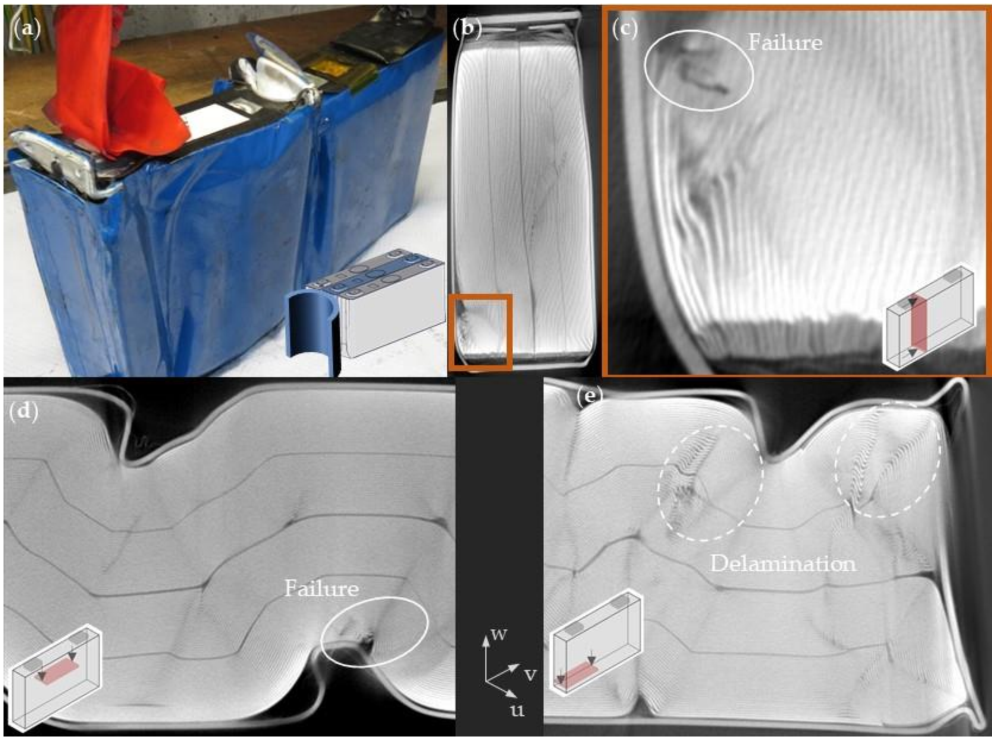

Figure 15. V-direction with cylindrical impactor: (**a**) deformed middle cell; (**b**–**e**) CT-Scans.

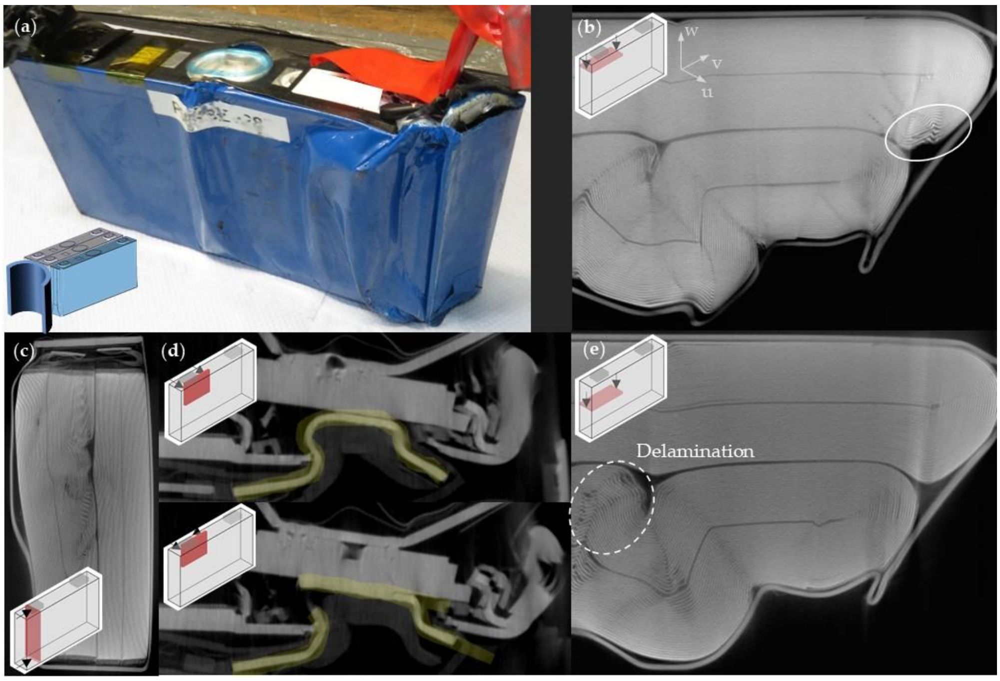

Figure 16. V-direction with cylindrical impactor: (**a**) deformed right cell; (**b**–**e**) CT-Scans.

The abuse tests were also conducted in w-direction, first with a hemispherical impactor. The deformed cell and CT-Scans from the middle cell are shown in Figure 17. Figure 17b,c illustrates the CT-Scans in the uw-plane, where only delamination of several electrodes' layers can be seen, but there is no sign of a crack in the electrodes. On the other hand, the casing of the middle cell shown in Figure 17 was plastically deformed, but the plastic material between the casing and the upper part of the jellyroll remained intact, which resulted in disappearance of a short circuit event. It is assumed that the first electrode failure will occur in the upper part of the jellyroll where a plastic component is pushed against the jellyroll layers.

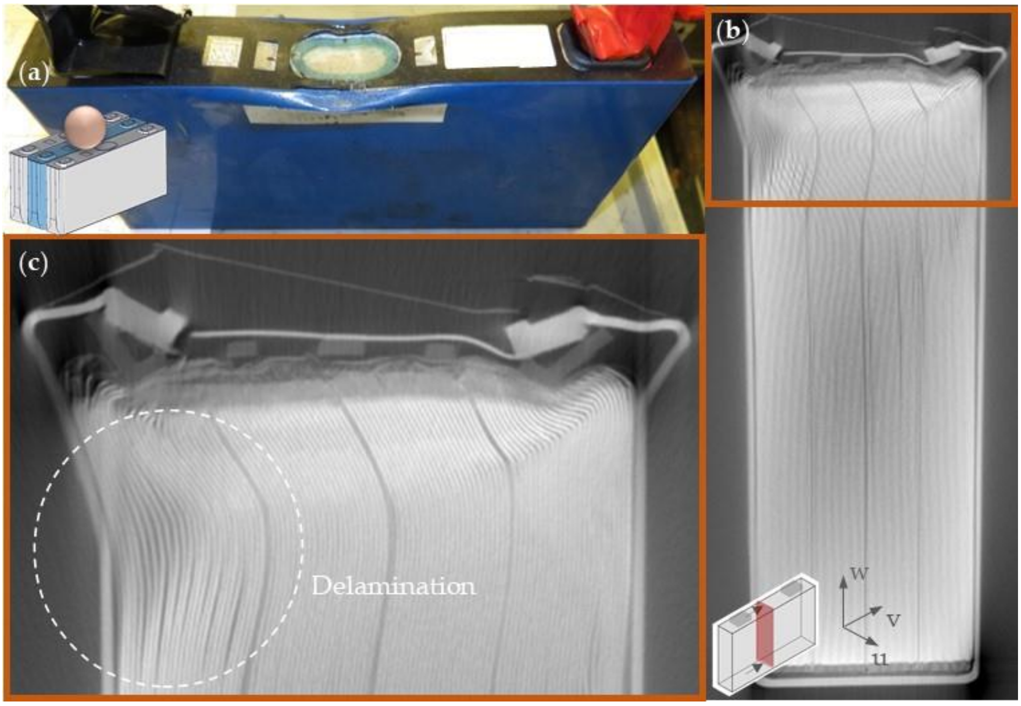

Figure 17. W-direction with hemispherical impactor: (**a**) deformed middle cell; (**b**,**c**) CT-Scans.

Finally, CT-Scans of the cylindrical test in the w-direction were investigated, as Figure 18 contains different cross-sections of the middle cell involved in the abuse testing. Initially, the cross-section in the uv-plane illustrates in Figure 18d–e rupture within some layers of the jellyrolls. Similar to the deformed cell in Figure 18a, the cross-sections in Figure 18b,c show the significant damage of the battery cell casing. In addition, the difference between casing deformation and jellyroll deformation can be seen. As expected, the failure of the electrodes is quite noteworthy, as the crack propagated through the layers of electrodes.

The failure of the electrodes layers in the middle cell has augmented the importance of the CT-Scans investigation of the left cell of the battery stack involved in the w-directional cylindrical compression test. Therefore, similar locations were selected as for the middle cell and a similar kind of revelation can be observed in Figure 19. The layers of electrodes in the left cell were also damaged at several locations. In addition, delamination of jellyroll layers and great deformation of the cell casing is quite evident.

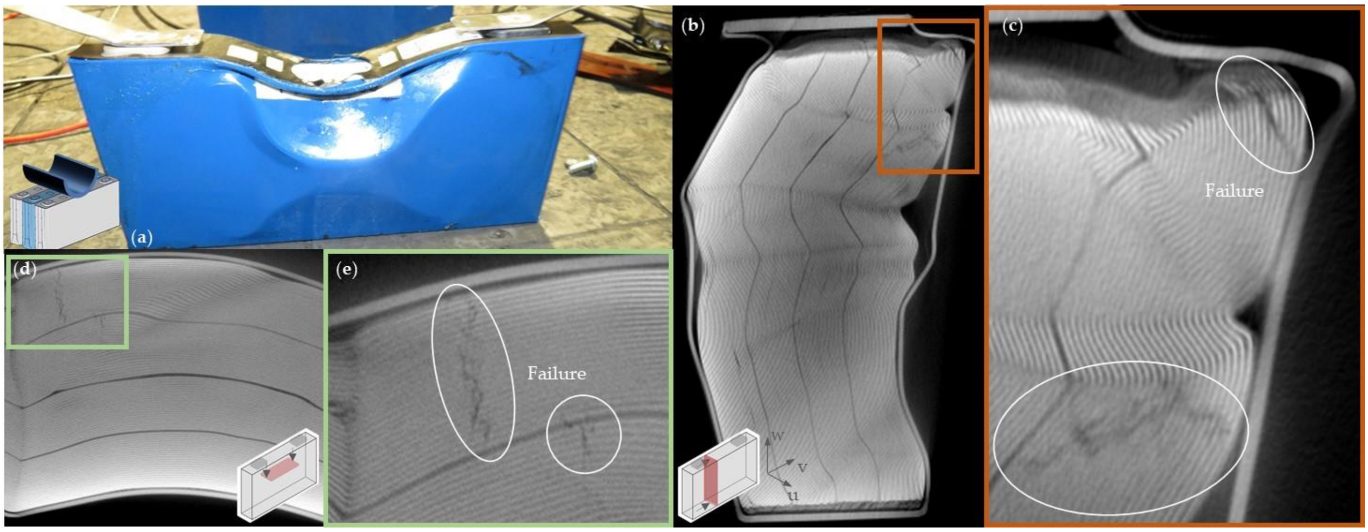

Figure 18. W-direction with cylindrical impactor: (**a**) deformed middle cell; (**b**–**e**) CT-Scans.

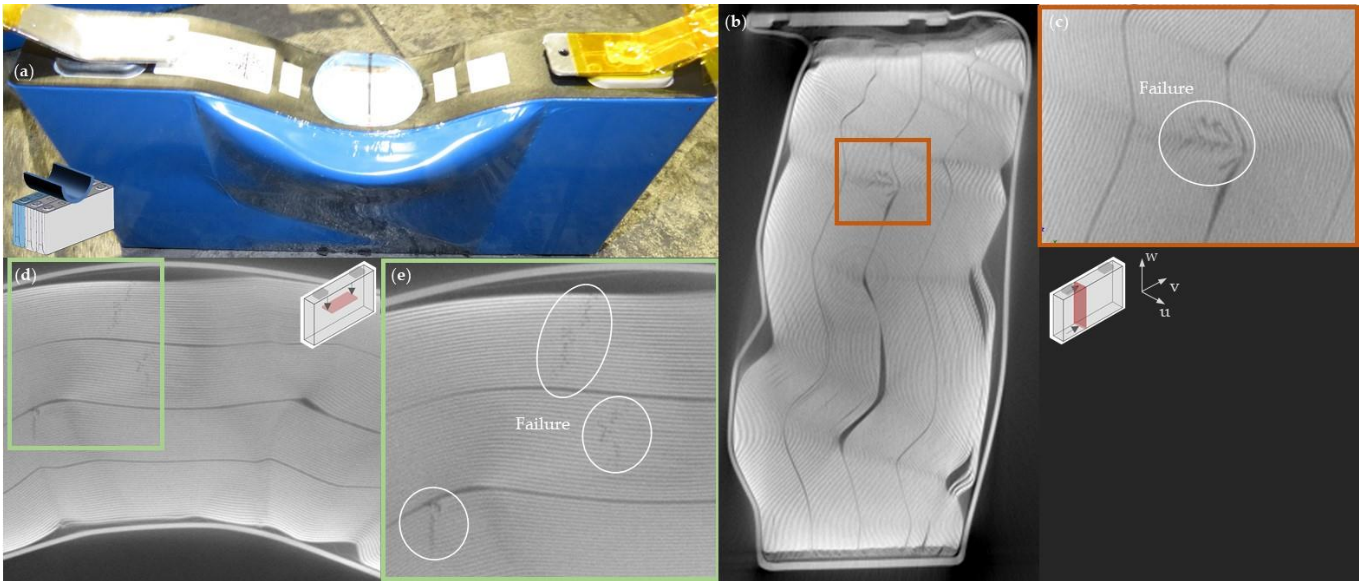

Figure 19. W-direction with cylindrical impactor: (**a**) deformed left cell; (**b**–**e**) CT-Scans.

4. Discussion

The results of the cell tests correspond in part to the results of previously published studies. In [1,22,27], a change in the curve for a cell under out-of-plane loading was also determined and the causes analyzed. When evaluating the test results in u-direction, it was also noticed that the scatter of the tests was very small. The cells used for these investigations were of an advanced prototype status. In [1], it was recognized that the degree of maturity of a cell has an influence on the scatter of the measurement results. The closer a cell is to the series level, the lower the scatter of the measurement results. Automated processes in series production can be cited as a reason for this.

A three-point bending was already carried out in [2] with a pouch cell. In this investigation, it was found that the layers slid off each other and thus the load hardly increased. The same is assumed for the results presented in this paper. With three-point bending, significantly higher intrusions could be achieved until an event occurred. It is suspected that the layers of the jellyroll also slide apart from each other in the prismatic cells used here, thus allowing a higher intrusion. Compared to the pouch cell format, it is assumed that the stiffer casing for prismatic cells contributes to a higher bending stiffness.

Another observation from the test results was the course of the cell voltage. In u-direction, the test with hemispherical impactor showed that the cell voltage initially drops, but then recovers somewhat and only then drops completely. In total, it takes about one time period for the cell voltage to drop entirely. In contrast, it was shown in Figure 4 that the cell voltage drops completely within a few seconds for the load case with cylindrical impactor in u-direction. For the results in v- and w-directions (see Figures 6 and 10), the cell voltage did not drop abruptly, but dropped continuously without recovery. This different behavior was also found in other investigations [15,28,29]. In [17], it was found that the drop in the cell voltage is firstly initiated by the components touching each other, which causes a short circuit. Depending on which components are in contact, there is a slow drop (see Figure 6) or a fast drop (see Figure 4). According to [17], the further progress depends on whether one of the current collectors or the separator foils melts first. If one of the current collector foils melts, a soft short circuit occurs, in which the cell voltage recovers somewhat (see Figure 3). If, however, one of the separator foils melts, a hard short circuit occurs, in which the cell voltage drops very quickly (see Figure 4).

During the tests in v- and w-directions, it was noticeable that one of the outer cells always failed first. After reviewing the CT scans, it became clear that the loading situation of the individual cells in a cell stack can differ significantly. Additionally, in these experiments, it was found that the time duration between the first event in one of the outer cells and the second event in the neighboring cell ranged from the 0.5 time period to the 37 time period. The large difference between the times can be explained by the environments. The large duration of the 37 time period was measured in the experiment with cylindrical impactor in w-direction. Here, the lateral support of the cells was not continuous to allow the cylindrical impactor to enter the cell stack. It is assumed that this allows the temperature to be dissipated better to the atmosphere, so that the neighboring cells do not heat up so quickly.

Another aspect of this investigation was the influence of the impactor shape on the intrusion tolerance until event. All directions were tested with a hemispherical and a cylindrical impactor with a diameter of 100 mm. For the tests in w-direction, the results cannot be directly compared because the supports of the cell stack were different. While in the tests with hemispherical impactor the lateral support was continuous, for the cylindrical impactor, the support had to be interrupted so that the cylinder could enter the cell stack. In u-direction, the results showed that a slightly lower intrusion to the event was possible with the cylindrical impactor compared to the hemispherical impactor. This is consistent with the study [30], where the intrusion up to an event was also slightly lower with a cylindrical impactor than with a hemispherical impactor.

For the v-direction, on the other hand, the results showed that, with a cylindrical impactor, the intrusion until event is approximately twice as large as with a hemispherical impactor. Based on the CT-scan results, it was demonstrated that the hemispherical impactor loads the jellyroll differently than the cylindrical impactor and that the load of the hemispherical impactor causes a tensile load on the jellyroll only in the upper region of the cell, which does not occur with the cylindrical impactor.

5. Conclusions and Outlook

In this study, cell tests were performed in all spatial directions with a hemispherical and a cylindrical impactor. In the out-of-plane direction, only one cell was tested at a time. The cell was either pushed against a rigid support or was subjected to three-point bending. In the two in-plane directions, a test always includes a stack of three cells. This was done to investigate the influence of impactor shape and support on the intrusion tolerance as well as the behavior of a stack of cells. The results lead to the following conclusions:

1. By isolating the impactor, it can be excluded as the cause of a short circuit during a crush test.
2. In the out-of-plane direction, a short-circuit is significantly more likely to occur under compression load (rigid support) compared to three-point bending.

3. The experiments in both in-plane directions demonstrate that the outer cells of a cell stack should always be analyzed as well, since they can be loaded differently, so that the intrusion tolerance is lower than for the cell targeted by the impactor. This is illustrated by the CT-scans, which revealed significantly more cracks in the outer cells of a cell stack.
4. The two impactor shapes used (spherical and cylindrical impactor) show that the load on a cell and thus the intrusion tolerance also differ significantly with the impactor shape. Therefore, different impactor shapes should always be tested during compression tests of a cell stack.
5. Even in tests that were stopped before a critical intrusion and in which no change in cell voltage was observed in the measurement data, cracks in the jellyroll have been detected in the CT evaluation of the cells involved. This finding can help to better predict a critical load of a cell and is an important foundation for an appropriate simulation model.
6. Thermal propagation in a cell stack depends strongly on the environment. The better the heat can be dissipated, the longer the propagation of the thermal runaway to another cell will take.

The tests in this study were all performed quasi-statically at a velocity of 1 mm/s. Further investigations could use much higher velocities to test the influence of strain rate dependence. In addition, the CT scans in this work were performed on deformed cells before an event. In order to observe not only cracks but also crack propagation, an in situ measurement would be necessary. Finally, the tested cells could be dissected in a post-mortem analysis. This would make it possible to determine which layers in the jellyroll are still intact and which have already failed. The results and findings of this work also provide the foundation for a mechanical simulation model that reproduces the behavior at the cell level. The results, opinions and conclusions expressed in this publication are not necessarily those of Volkswagen Aktiengesellschaft.

Author Contributions: Conceptualization, S.S.; methodology, S.S. and P.B.; formal analysis, S.S. and P.B.; investigation, S.S.; resources, S.S.; writing—original draft preparation, S.S and M.A.R.S.; writing—review and editing, S.S. and M.A.R.S.; visualization, S.S.; supervision, T.V. All authors have read and agreed to the published version of the manuscript.

Funding: We acknowledge support by the German Research Foundation and the Open Access Publication Funds of Technische Universität Braunschweig.

Data Availability Statement: Due to confidentiality of prototype test data, much data in this research are normalized and would not be shared. All force, displacement and temperature data of the battery cell tests are shown without numeric values. Even without precise numerical values, the key messages of this publication are valid, as the key messages refer only to content and not to specific numerical values.

Acknowledgments: S.S. would like to thank Christoph Zorn and Ulf Bunge at Volkswagen AG for their support and constructive comments.

Conflicts of Interest: The authors declare no conflict of interest.

References

1. Kotter, P.; Kisters, T.; Schleicher, A. Dynamic impact tests to characterize the crashworthiness of large-format lithium-ion cells. *J. Energy Storage* **2019**, *26*, 100948. [CrossRef]
2. Sahraei, E.; Hill, R.; Wierzbicki, T. Calibration and finite element simulation of pouch lithium-ion batteries for mechanical integrity. *J. Power Sources* **2012**, *201*, 307–321. [CrossRef]
3. Pan, Z.; Li, W.; Xia, Y. Experiments and 3D detailed modeling for a pouch battery cell under impact loading. *J. Energy Storage* **2020**, *27*, 101016. [CrossRef]
4. Zhu, J.; Koch, M.M.; Lian, J.; Li, W.; Wierzbicki, T. Mechanical Deformation of Lithium-Ion Pouch Cells under In-Plane Loads—Part I. *J. Electrochem. Soc.* **2020**, *167*, 90533. [CrossRef]
5. Ali, M.Y.; Lai, W.-J.; Pan, J. Computational models for simulations of lithium-ion battery cells under constrained compression tests. *J. Power Sources* **2013**, *242*, 325–340. [CrossRef]

6. Zhu, J.; Li, W.; Xia, Y.; Sahraei, E. Testing and Modeling the Mechanical Properties of the Granular Materials of Graphite Anode. *J. Electrochem. Soc.* **2018**, *165*, A1160–A1168. [CrossRef]
7. Wang, L.; Yin, S.; Zhang, C.; Huan, Y.; Xu, J. Mechanical characterization and modeling for anodes and cathodes in lithium-ion batteries. *J. Power Sources* **2018**, *392*, 265–273. [CrossRef]
8. Zhu, J.; Zhang, X.; Luo, H.; Sahraei, E. Investigation of the deformation mechanisms of lithium-ion battery components using in-situ micro tests. *Appl. Energy* **2018**, *224*, 251–266. [CrossRef]
9. Zhang, C.; Xu, J.; Cao, L.; Wu, Z.; Santhanagopalan, S. Constitutive behavior and progressive mechanical failure of electrodes in lithium-ion batteries. *J. Power Sources* **2017**, *357*, 126–137. [CrossRef]
10. Bonatti, C.; Mohr, D. Anisotropic viscoplasticity and fracture of fine grained metallic aluminum foil used in Li-ion batteries. *Mater. Sci. Eng. A* **2016**, *654*, 329–343. [CrossRef]
11. Jiang, X.; Luo, H.; Xia, Y.; Zhou, Q. Mechanical Behavior of Lithium-Ion Battery Component Materials and Error Sources Analysis for Test Results. *SAE Int. J. Mater. Manf.* **2016**, *9*, 614–621. [CrossRef]
12. Luo, H.; Zhu, J.; Sahraei, E.; Xia, Y. Adhesion strength of the cathode in lithium-ion batteries under combined tension/shear loadings. *RSC Adv.* **2018**, *8*, 3996–4005. [CrossRef]
13. Sahraei, E.; Meier, J.; Wierzbicki, T. Characterizing and modeling mechanical properties and onset of short circuit for three types of lithium-ion pouch cells. *J. Power Sources* **2014**, *247*, 503–516. [CrossRef]
14. Chen, X.; Yuan, Q.; Wang, T.; Ji, H.; Ji, Y.; Li, L.; Liu, Y. Experimental study on the dynamic behavior of prismatic lithium-ion battery upon repeated impact. *Eng. Fail. Anal.* **2020**, *115*, 104667. [CrossRef]
15. Zhu, X.; Wang, H.; Wang, X.; Gao, Y.; Allu, S.; Cakmak, E.; Wang, Z. Internal short circuit and failure mechanisms of lithium-ion pouch cells under mechanical indentation abuse conditions: An experimental study. *J. Power Sources* **2020**, *455*, 227939. [CrossRef]
16. Ren, F.; Cox, T.; Wang, H. Thermal runaway risk evaluation of Li-ion cells using a pinch–torsion test. *J. Power Sources* **2014**, *249*, 156–162. [CrossRef]
17. Liu, B.; Jia, Y.; Yuan, C.; Wang, L.; Gao, X.; Yin, S.; Xu, J. Safety issues and mechanisms of lithium-ion battery cell upon mechanical abusive loading. *Energy Storage Mater.* **2020**, *24*, 85–112. [CrossRef]
18. Hess, S.; Wohlfahrt-Mehrens, M.; Wachtler, M. Flammability of Li-Ion Battery Electrolytes. *J. Electrochem. Soc.* **2015**, *162*, A3084–A3097. [CrossRef]
19. Feng, X.; Ouyang, M.; Liu, X.; Lu, L.; Xia, Y.; He, X. Thermal runaway mechanism of lithium ion battery for electric vehicles. *Energy Storage Mater.* **2018**, *10*, 246–267. [CrossRef]
20. Deng, J.; Smith, I.; Bae, C.; Rairigh, P.; Miller, T.; Surampudi, B.; L'Eplattenier, P.; Caldichoury, I. Impact Modeling and Testing of Pouch and Prismatic Cells. *J. Electrochem. Soc.* **2020**, *167*, 90550. [CrossRef]
21. Zheng, W.-J.; Lan, F.-C.; Chen, J.-Q.; Li, Z.-J. Compression Experiment and Simulation on Prismatic Lithium-ion Batteries. *DEStech Trans. Environ. Energy Earth Sci.* **2017**, 393–403. [CrossRef]
22. Zhu, L.; Ge, Y.; Wang, L.; Zhang, L.; Liu, Y.; Xia, Y. Mechanical Anisotropy and Strain-Rate Dependency of a Large Format Lithium-Ion Battery Cell: Experiments and Simulations. In *SAE WCX Digital Summit*; SAE International, 400 Commonwealth Drive: Warrendale, PA, USA, 2021.
23. Xiao, F.; Xing, B.; Xia, Y. Mechanical Response of Laterally-Constrained Prismatic Battery Cells under Local Loading. In *WCX SAE World Congress Experience*; SAE International, 400 Commonwealth Drive: Warrendale, PA, USA, 2020.
24. Deng, J.; Smith, I.; Bae, C.; Rairigh, P.; Miller, T.; Surampudi, B. Communication—Impact Behaviors of Pouch and Prismatic Battery Modules. *J. Electrochem. Soc.* **2021**, *168*, 20520. [CrossRef]
25. Zhu, F.; Lei, J.; Du, X.; Currier, P.; Gbaguidi, A.; Sypeck, D. Crushing Behavior of Vehicle Battery Pouch Cell and Module. *SAE Int. J. Mater. Manf.* **2018**, *11*, 341–348. [CrossRef]
26. Kalnaus, S.; Wang, H.; Watkins, T.R.; Kumar, A.; Simunovic, S.; Turner, J.A.; Gorney, P. Effect of packaging and cooling plates on mechanical response and failure characteristics of automotive Li-ion battery modules. *J. Power Sources* **2018**, *403*, 20–26. [CrossRef]
27. Li, W.; Zhu, J. A Large Deformation and Fracture Model of Lithium-Ion Battery Cells Treated as a Homogenized Medium. *J. Electrochem. Soc.* **2020**, *167*, 120504. [CrossRef]
28. Yang, S.; Wang, W.; Lin, C.; Shen, W.; Li, Y. Investigation of Internal Short Circuits of Lithium-Ion Batteries under Mechanical Abusive Conditions. *Energies* **2019**, *12*, 1885. [CrossRef]
29. Maleki, H.; Howard, J.N. Internal short circuit in Li-ion cells. *J. Power Sources* **2009**, *191*, 568–574. [CrossRef]
30. Chung, S.H.; Tancogne-Dejean, T.; Zhu, J.; Luo, H.; Wierzbicki, T. Failure in lithium-ion batteries under transverse indentation loading. *J. Power Sources* **2018**, *389*, 148–159. [CrossRef]